


Research Article

Analysis of the Shear Capacity of Ultrahigh Performance Concrete Beams Based on the Modified Compression Field Theory

Wei Feng,^{1,2} Hongming Feng ,¹ Zhijun Zhou,¹ and Xiongwei Shi²

¹School of Highway, Chang'an University, Xi'an, Shaanxi 710064, China

²Xi'an Highway Research Institute Co. Ltd., Xi'an, Shaanxi 710065, China

Correspondence should be addressed to Hongming Feng; fenghongming@chd.edu.cn

Received 20 January 2021; Revised 5 May 2021; Accepted 5 June 2021; Published 17 June 2021

Academic Editor: Luigi Di Sarno

Copyright © 2021 Wei Feng et al. This is an open access article distributed under the Creative Commons Attribution License, which permits unrestricted use, distribution, and reproduction in any medium, provided the original work is properly cited.

An analysis model of the shear capacity of prestressed ultrahigh performance concrete (UHPC) beams under the combined action of bending and shearing was established in this paper based on the modified compression field theory and by considering the unique material constitutive relation of UHPC. Shear tests were performed using three prestressed UHPC-T beams with different shear-span ratios to verify the correctness of the model. The results showed that the shear-span ratio greatly influenced the shear capacity and failure modes of UHPC-T beams. Upon increasing the shear-span ratio, the failure modes of the three beams were inclined compression failure, shear compression failure, and diagonal tension failure, successively. When the shear-span ratio changed from 1.04 to 2.12, the shear bearing capacity decreased greatly; however, when the shear-span ratio changed from 2.12 to 3.19, the decrease of the shear bearing capacity was very small. In addition, the MCFT analysis model was used to analyze the experimental data, and the predicted results were in good agreement, which proved the applicability of the model. Finally, according to the existing shear test results of UHPC beams and based on the main influencing factors, a simplified formula for predicting the shear capacity of UHPC beams was obtained by fitting. Comparing the MCFT model with the results of other pieces of literature, this formula accurately predicted the shear capacity of UHPC beams. The MCFT model and the simplified formula presented in this paper provide a powerful tool for predicting the shear performance of UHPC-T beams, which will contribute to the design and analysis of UHPC-T beams.

1. Introduction

Ultrahigh performance concrete (UHPC) is a new type of steel fiber-reinforced cement-based composite material with many excellent properties [1–3], including superhigh strength, high ductility, good durability, and resistance to environmental degradation [4–7]. Because of these excellent properties, UHPC has been widely used in bridge engineering, structure repair, and other fields [8–12]. The application of UHPC in bridge engineering can greatly reduce the weight of bridge structures and maintenance times, which help extend the service life of bridges and reduce costs [13, 14].

With increasing in-depth research and applications of UHPC in engineering, scholars have carried out a series of studies on the shear performance of UHPC structures. Voo

et al. [15, 16] conducted 16 prestressed UHPC I-beam tests successively and found that the number and type of fibers had no significant effect on the cracking load, but increasing the fiber volume increased the failure load. Based on the plastic theory, the PSM-VEM model was proposed, which assumed that the critical crack ran through the whole beam height and was unaffected by the shear compression zone. A comparison with the test results showed that the model was suitable for the shear calculation of UHPC beams. Ngo et al. [17] used a self-developed shear test system to study the shear performance of UHPFRC. The results showed that the shear performance of UHPC was affected by the shear-span ratio and fiber volume, as well as the tensile strength. Higher shear-span ratios promoted lower shear strengths, while higher fiber volumes promoted higher shear strengths. According to the results, a theoretical prediction model of

shear strength of UHPC considering the tensile strength and shear-span ratio was proposed. Ji et al. [18, 19] conducted shear tests on 12 RPC-T beams. The experimental results showed that the ultimate shear capacity of the beams increased upon increasing the stirrup ratio and longitudinal reinforcement ratio and decreased upon increasing the shear-span ratio. According to the results, the softening coefficient was corrected to establish the truss model, and the shear performance of RPC beams was predicted. The above calculation methods of UHPC shear capacity used different theories to explain the shear failure mechanism of the structure from different perspectives [20–23]; however, the shear-span ratio is not fully considered by the limit equilibrium theory. The analysis accuracy of specimens with a shear-span ratio of 2 that undergo shear-pressure failure is relatively high, while it is relatively low for specimens with a small shear span. The plasticity theory primarily considers the influence of compressive strength and horizontal projected length of the main diagonal crack, but it does not consider the influence of stirrups, longitudinal reinforcement, or prestress on the shear capacity. Although the truss model provides a simple calculation method and clear concept, the theory does not conform to the deformation compatibility condition and cannot describe the whole shear stress process.

Due to the deficiency of the above theoretical model, Vecchio and Collins proposed the modified compression field theory [24, 25], which considers the influence of shear-span ratio, stirrup ratio, prestress, and steel fiber on shear bearing capacity, and it has been adopted by Canadian and American codes [26, 27]. Its main feature is the decomposition of the shear problem of the combined bending-shearing force state into pure shear and pure bending states, which are analyzed separately and then calculated by superposition. On this basis, Crane [28] predicted the shear capacity of six composite beams (UHPC I-beam at the bottom and HPC panel at the top) by using the modified compression field theory after considering the contribution of steel fiber. Liang and Wang [29] proposed an improved MCFT calculation model based on the modified compression field theory by considering the pin bolt effect of longitudinal bars and calculated the shear performance of UHPC beams. Baby et al. [30] used a hyperbolic model to characterize the compression constitutive model of UHPC and discussed the feasibility of applying the MCFT theory to evaluate the shear performance of prestressed ultrahigh performance reinforced concrete beams; however, in that current study, the constitutive model used to analyze the pure bending state was generally obtained by scaling based on the ordinary concrete constitutive model, which cannot clearly reflect the force characteristics of the UHPC material, leading to errors in the results.

This paper aims to establish an analysis model for the shear capacity of UHPC beams based on the modified compression field theory. Considering the unique constitutive relation of UHPC materials, an improved analysis model was established and verified by experiments. A

comparison of the results from codes and experiments showed that the existing shear strength formula is not suitable for predicting the shear capacity of UHPC-T beams; therefore, according to the MCFT model and the existing test results, a simplified prediction formula for the shear capacity of UHPC beams was obtained by fitting. The research results provide a practical calculation method for the shear design of UHPC beams and also provide a deeper understanding of the shear performance of UHPC-T beams.

2. Calculation Model Based on MCFT

The modified compression field theory was used to establish the strain compatibility equation and stress balance equation based on material mechanics and then combined with the UHPC constitutive relations to obtain the calculation method of the shear bearing capacity according to three convergence conditions.

2.1. Basic Assumptions. The basic assumptions of the MCFT are as follows:

- (a) The shear stress and normal stress of the concrete microelement body are uniformly distributed when it is under load
- (b) The stress-strain of concrete is the average stress-strain of the cracked area
- (c) The principal stress direction of concrete is the same as the principal strain direction
- (d) Reinforced concrete does not experience bond-slip between each other, and there is an ideal bond between them
- (e) The axial stress of reinforcement is the only considered factor, and the reinforcement shear stress is not considered

2.2. Strain Coordination Equation. According to the basic assumption, assuming that the UHPC and the reinforcing bar are in an ideal bonding state, and without considering the shear stress of the reinforcing bar, equations (1) and (2) can be obtained:

$$\varepsilon_{cx} = \varepsilon_{sx} = \varepsilon_x, \quad (1)$$

$$\varepsilon_{cy} = \varepsilon_{sy} = \varepsilon_y, \quad (2)$$

where ε_{cx} and ε_{cy} represent the strain of UHPC in the x and y -directions, respectively, ε_{sx} and ε_{sy} represent the strain of the reinforcement in the x and y -directions, respectively, and ε_x and ε_y represent the average strain of the reinforced concrete microelements in the x and y -directions, respectively.

The average strain of the reinforced concrete microelements conforms to Mohr's circle for strain. According to the geometric conditions in Figure 1, equations (3)–(5) can be obtained:

$$\varepsilon_x = \frac{\varepsilon_1 \tan^2 \theta + \varepsilon_2}{1 + \tan^2 \theta}, \quad (3)$$

$$\tan^2 \theta = \frac{\varepsilon_x - \varepsilon_2}{\varepsilon_y - \varepsilon_2}, \quad (4)$$

$$\varepsilon_1 = \varepsilon_x + \varepsilon_y - \varepsilon_2. \quad (5)$$

Combining equations (4) and (5), the average strain in the x -direction (ε_x) and y -direction (ε_y) can be obtained, as shown in equations (6) and (7):

$$\varepsilon_x = \frac{\varepsilon_1 \tan^2 \theta + \varepsilon_2}{1 + \tan^2 \theta}, \quad (6)$$

$$\varepsilon_y = \frac{\varepsilon_1 + \varepsilon_2 \tan^2 \theta}{1 + \tan^2 \theta}, \quad (7)$$

where ε_1 and ε_2 represent the principal tension strain and principal compressive strain of reinforced concrete, respectively, and θ represents the principal compressive strain angle of the concrete.

2.3. Stress Balance Equation. According to the basic assumption, the average stress and average strain of concrete after cracking conform to Mohr's circle for stresses. Equation (8) can be obtained from Figure 2.

$$f_1 + f_2 = v(\tan \theta + \cot \theta), \quad (8)$$

where f_1 and f_2 represent the main tensile stress and the main compressive stress, respectively, and v is the average shear stress of the section.

Figure 3 shows the analysis model of a UHPC beam based on MCFT. As shown in Figure 3(a), equation (9) can be obtained:

$$V = b_w h_0 v, \quad (9)$$

where V is the shear force of the beam, b_w represents the width of the web, and h_0 represents the effective height of the section.

Considering the balance of forces in the vertical direction, equation (10) can be obtained from Figure 3(b):

$$A_{sv} f_v = (f_2 \sin^2 \theta - f_1 \cos^2 \theta) b_w s, \quad (10)$$

where A_{sv} and f_v represent the stirrup area and stirrup stress, respectively, and s is the stirrup spacing.

From equations (8)–(10), the following equation can be obtained:

$$V = f_1 b_w h_0 \cot \theta + \frac{A_{sv} f_v}{s} h_0 \cot \theta. \quad (11)$$

Considering the balance of forces in the horizontal direction and combining with equations (8) and (12) can be obtained from Figure 3(b):

$$F'_C = V \cot \theta - f_1 b_w h_0, \quad (12)$$

where F'_C represents the axial resultant force of the longitudinal reinforcement in the horizontal direction of the section.

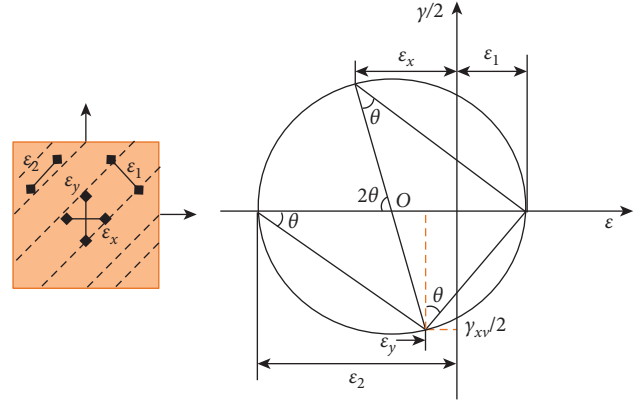


FIGURE 1: Mohr's circle for average strain.

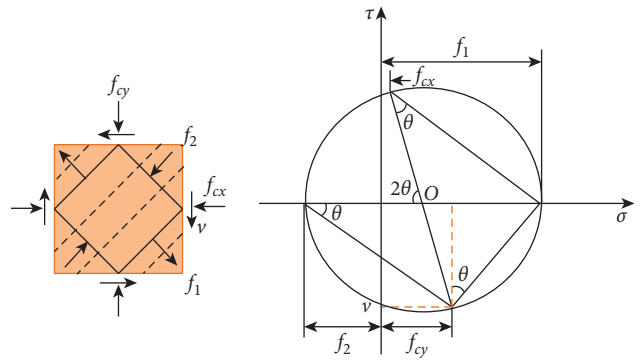


FIGURE 2: Mohr's circle for average stresses.

2.4. Material Constitutive Relationship. Based on the strain coordination equation and stress balance equation, the constitutive models of ordinary steel bars, prestressed steel bars, and UHPC are introduced to establish the equation group.

2.4.1. Ordinary Steel Bars Constitutive Model. It is assumed that the stress-strain relationship of the ordinary steel bars constitutive model is an ideal elastoplastic relationship as follows:

$$f_s = \begin{cases} E_s \varepsilon_x, & \varepsilon_x \leq \varepsilon_n, \\ f_y, & \varepsilon_x > \varepsilon_n, \end{cases} \quad (13)$$

where f_y and ε_n represent the yield stress and the strain of the steel bar, respectively, and E_s represents the elastic modulus.

2.4.2. Prestressed Steel Bars Constitutive Model. The constitutive relationship of prestressed steel bars is expressed in two stages, as follows:

$$f_s = \begin{cases} E_p \varepsilon_p, & \varepsilon_p \leq \varepsilon_{p0}, \\ E_p \varepsilon_p \left[1 + \left(\frac{E_p \varepsilon_p}{f_{pu}} \right)^{4.38} \right]^{-1/4.38}, & \varepsilon_x \leq \varepsilon_n, \end{cases} \quad (14)$$

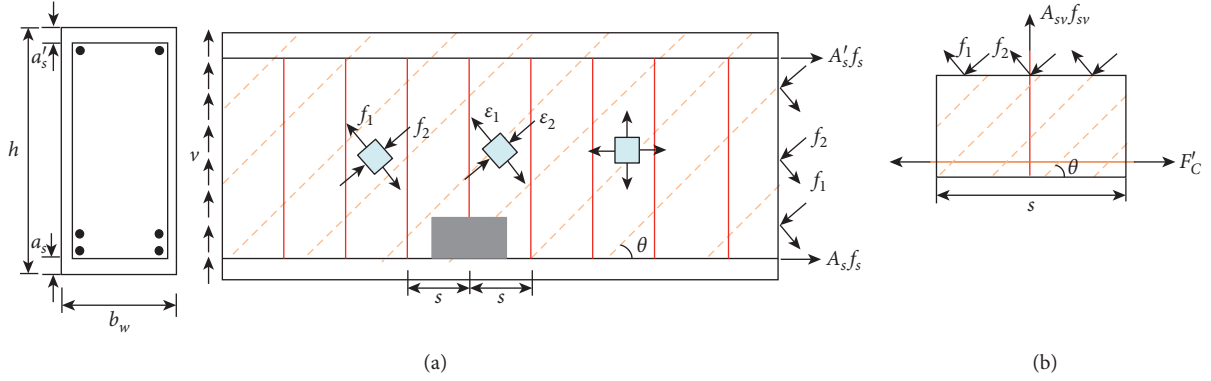


FIGURE 3: Analysis model of a UHPC beam based on MCFT. (a) Principal stress of UHPC; (b) equilibrium of UHPC element forces.

where E_p , ϵ_p , ϵ_{p0} , and f_{pu} represent the elastic modulus, strain, proportional limit strain, and ultimate strength, respectively. The initial strain of the prestressed steel bars after tensioning is $\epsilon_{pi} = f_{pi}/E_p$; therefore, the initial strain of the prestressed reinforcement component should be considered during calculation.

2.4.3. UHPC Constitutive Model. Concrete is in the biaxial stress state and the uniaxial stress state, respectively, when considering the pure shear and pure bending stress states; therefore, the constitutive relationship for these two different stress states should be selected separately.

(1) *Biaxial Stress State.* The compression constitutive model of UHPC under biaxial stress state refers to the softening constitutive model of ordinary concrete and is scaled in equal proportion, as shown in Figure 4.

The constitutive relationship of UHPC compression under biaxial stress is described by

$$f_{c2} = f_{c2\max} \left[2 \left(\frac{\epsilon_2}{\epsilon_0} \right) - \left(\frac{\epsilon_2}{\epsilon_0} \right)^2 \right], \quad (15)$$

$$\frac{f_{c2\max}}{f'_c} = \frac{1}{0.8 - 0.34\epsilon_1/\epsilon_0}, \quad (16)$$

where ϵ_0 , ϵ_1 , ϵ_2 , f'_c , and $f_{c2\max}$, respectively, represent the peak uniaxial compressive strain, the main tensile strain, the main compressive strain, the uniaxial compressive strength, and the ultimate compressive strength of UHPC.

The tensile constitutive model of UHPC under the biaxial stress state is shown in Figure 5, and the tensile constitutive relationship of UHPC is described by equation (17): where f_{cr} represents the tensile strength and f_{tu} represents the residual tensile stress after UHPC cracking. In this paper, $f_{tu} = 0.75f_{cr}$.

$$f_t = \begin{cases} E_c \epsilon_1, & \epsilon_1 \leq \epsilon_{cr}, \\ \frac{f_{cr} + \beta f_{tu}}{0.005}, & \epsilon_1 > \epsilon_{cr}, \end{cases} \quad (17)$$

$$\beta = \sqrt{\frac{\epsilon_1 - \epsilon_{cr}}{0.005}}, \quad (18)$$

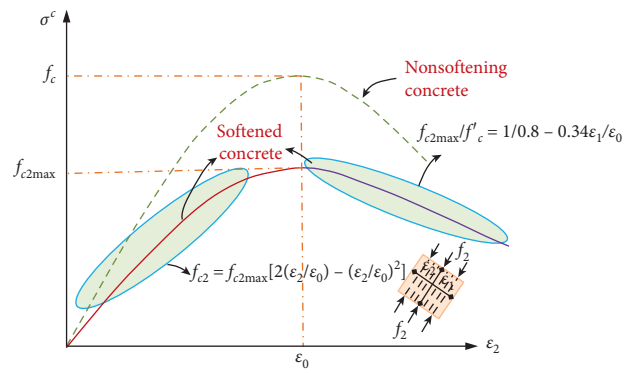


FIGURE 4: Compression constitutive model of UHPC in the biaxial stress state.

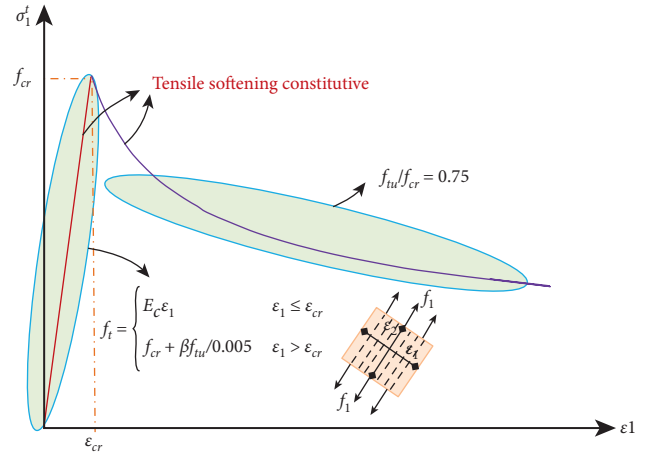


FIGURE 5: Tensile constitutive model of UHPC in the biaxial stress state.

(2) *Uniaxial Stress State.* The constitutive relationship of UHPC under uniaxial compression adopts the stress-strain relationship proposed by Yang and Fang [31], and the compression constitutive relationship of UHPC under the uniaxial stress state is shown in the following equation:

$$\sigma_c = \begin{cases} f_c \frac{n\xi - \xi^2}{1 + (n-2)\xi}, & \varepsilon \leq \varepsilon_0, \\ f_c \frac{\xi}{2(\xi-1)^2 + \xi}, & \varepsilon > \varepsilon_0, \end{cases} \quad (19)$$

where $\varepsilon_0 = 3500\mu\varepsilon$, $\xi = (\varepsilon/\varepsilon_0)$, $n = (E_c/E_g)$, E_c is the initial modulus of elasticity, and E_g is the secant modulus at the peak point of stress-strain curve.

The uniaxial tensile constitutive model of UHPC is based on the uniaxial tensile test results of UHPC provided by Zhang et al. [32] and a two-stage tensile constitutive relationship. Considering the contribution of UHPC tensile performance after cracking to shear resistance, the following improvements are made. The stress-strain relationship is adopted in the tensile strain hardening section, and the stress crack width relationship in the stress softening section is proposed by Li et al. [33], as shown in Figure 6.

The tensile constitutive relationship of UHPC under uniaxial stress state is shown in the following equation:

$$\sigma_t = \begin{cases} \frac{f_t}{\varepsilon_{t0}} \varepsilon, & \varepsilon \leq \varepsilon_{t0}, \\ f_t, & \varepsilon_{t0} < \varepsilon \leq \varepsilon_{tp}, \\ f_t \frac{1}{[1 + (\varepsilon - \varepsilon_{tp})l_c/w_p]^p}, & \varepsilon > \varepsilon_{tp}, \end{cases} \quad (20)$$

where p represents the test fitting parameter, w_p represents the crack width when the stress decreases, and $2^{-p}f_t$ and l_c denote the section characteristic length. For rectangular sections and T-sections, take $l_c = 2/3h$, where h is the height of the section.

2.5. Section Analysis of Bending-Shearing Composite Action.

In the section analysis of bending-shearing composite action, the test beam is analyzed separately according to pure bending and pure shear stress forms, and the corresponding UHPC constitutive models are used in the calculation.

2.5.1. Shear Analysis of Beams. In the shear analysis and calculations of the test beam, it is assumed that the shear force is uniformly distributed at the section height. Since the shear capacity of a T-shaped beam is affected by the flange width, the contribution of the flange plate to the shear bearing capacity is considered. In the calculation, the effective width of a T-shaped beam is taken as $b + 2h_f$, and the UHPC constitutive model used equations (15)–(18). The calculation section is shown in Figure 7. The longitudinal and transverse strains are calculated by (6) and (7), respectively. The vertical shear V is calculated by equation (11), and the horizontal component F'_c is calculated by equation (12).

2.5.2. Flexural Analysis of Beams. In the flexural analysis of beams, since ordinary concrete does not consider the strength of cracked concrete, the contribution of this part is

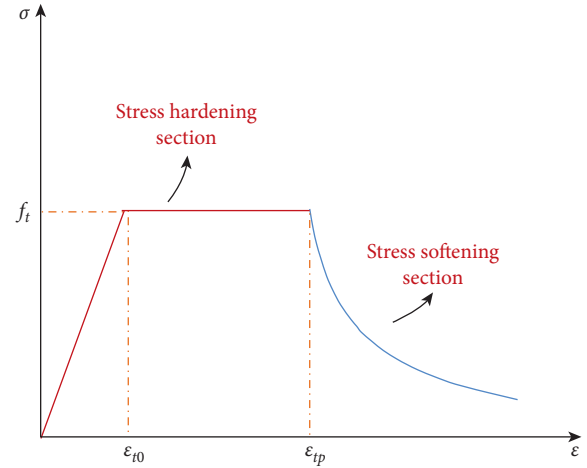


FIGURE 6: Uniaxial tensile constitutive model of UHPC.

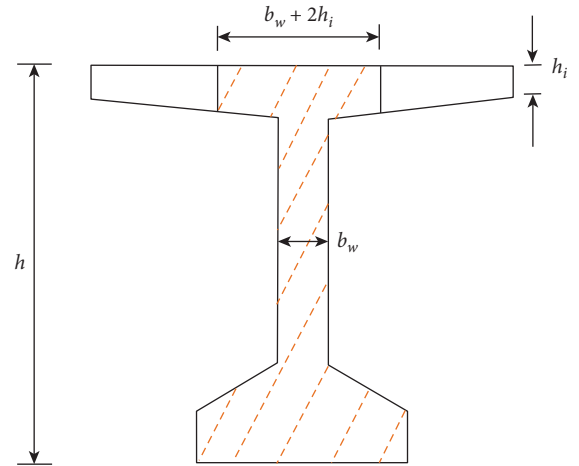


FIGURE 7: Shear section of the T-shaped beam.

not considered in the modified compression field theory; however, the residual tensile strength of UHPC beams after cracking cannot be ignored. Therefore, this paper introduces the improved UHPC tensile component, which is calculated by equations (19) and (20).

Figure 8 shows the stress-strain relationship under a pure bending moment. To perform an accurate calculation, this paper assumes that the shear stress is uniformly distributed. According to the strain simplified method proposed by Collins, the longitudinal strain at the half-height of the section is taken as the horizontal strain of the shear part during the calculation; therefore, the calculation of flexural resistance conforms to the assumption of a flat section, and the value of ε_x calculated by equation (6) in the shear analysis is regarded as the longitudinal strain at half the height of the section. According to the force balance conditions, equation (21) can be obtained:

$$F_c = \int_c \sigma_c b dx + \int_c \sigma_t b dx + A_p f_p + A_s f_y, \quad (21)$$

where σ_c and σ_t are the compressive and tensile stresses of the concrete, respectively, and A_p and A_s are the areas of the prestressed reinforcement and ordinary reinforcement, respectively.

The flexural capacity M_1 can be expressed by equation (22) as follows:

$$M_1 = \int_c \sigma_c y b dx + \int_t \sigma_t y b dx + A_p f_p y a_p + A_s f_y y_s, \quad (22)$$

where y_p and y_s are the positions of the prestressed reinforcement and ordinary reinforcement relative to the upper edge of the section, respectively.

2.6. Block Diagram of the Calculation Program. The main variables calculated in this paper are the section failure angle θ , stirrup stress f_v , and upper edge compressive strain ε_t of the bending calculation. To determine these variables, an initial principal tensile strain ε_1 can be considered, the values of the relevant variables are assumed, and the variables are solved via cyclic iteration. To determine the closed solution, three convergence criteria are required:

- Because stirrup stress is equal to the assumed value, the discriminant conditional expression (23) can be obtained.
- The discriminant conditional expression (24) can be obtained from the axial resultant force to zero.
- The discriminant conditional expression (25) can be obtained from the equal bending moment.

$$f_v = f_s(\varepsilon_y), \quad (23)$$

$$N = F'_C + F_C = 0, \quad (24)$$

$$M_1 = Va, \quad (25)$$

where F'_C and F_C are the horizontal axial forces in the shear-resistance and bending-resistance calculations, respectively, V and a are the shear force in the shear-resistance calculation and the distance of the actual position from the support, respectively, and M_1 is the bending moment in the bending-resistance calculation.

Combining the above deformation compatibility equation, stress balance equation, material constitutive relation, and three convergence discriminants, the MCFT-based calculation procedure of the shear bearing capacity of UHPC beam was compiled by MATLAB, as shown in Figure 9.

3. Model Test

3.1. Material Properties. UHPC adopts UA type with reference to the Swiss specification, with a designed compressive strength of 120 MPa and an elastic tensile strength of 7 MPa [34]. The main raw materials include cement, silica fume, quartz flour, quartz powder, superplasticizer, and water. The details are listed in Table 1, and the content

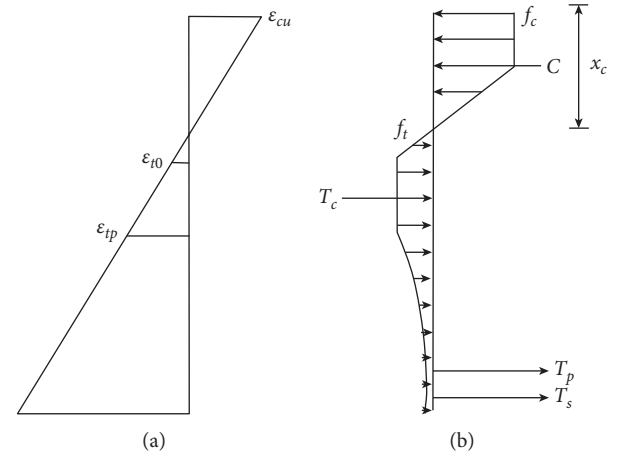


FIGURE 8: Stress-strain under the pure bending moment: (a) strain distribution; (b) stress distribution.

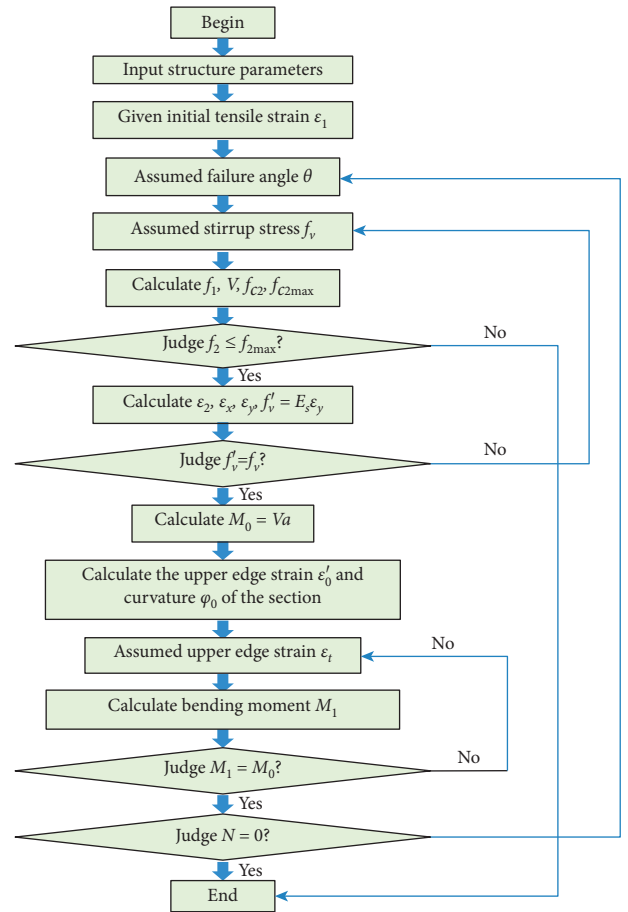


FIGURE 9: Block diagram of the calculation program.

of steel fiber was 2%. During the pouring of the test beam, six $100 \times 100 \times 100$ cube test blocks were made to test the compressive strength of the material, three $100 \times 100 \times 300$ prism test blocks were made to test the elastic modulus of the material, and three $100 \times 100 \times 400$ prism test blocks were made to test the flexural strength of the material. All the material test specimens were cured under the same

TABLE 1: Mix proportion of the UHPC matrix.

Component	Cement	Silica fume	Quartz flour	Quartz powder	Superplasticizer	Water
Mass ratio	1.000	0.250	1.100	0.300	0.019	0.2

TABLE 2: Mechanical properties of UHPC.

E_c	f_{cu}	f_{ct}
42.2 GPa	126 MPa	21.7 MPa

conditions as the test beam. The test results are shown in Table 2.

3.2. Test Specimens. The calculated spans of the three constructed prestressed UHPC-T beams were 1.4 m, 2.8 m, and 4.2 m, respectively, and the shear-span ratios were $\lambda = 1.6$, $\lambda = 2.12$, and $\lambda = 3.19$ respectively. The three test beams had the same cross section, the beam height was 0.6 m, the top plate width was 0.6 m, the lower edge width was 0.3 m, the web thickness was 70 mm, and the horseshoe edge height was 80 mm. The section and reinforcement arrangement of the test beam is illustrated in Figure 10. Two $\Phi 15.2-4$ prestressed steel strands were arranged in a horseshoe at the lower edge of the test beam, and the tensile stress was 1010 MPa. Five longitudinal bars with diameters of 12 mm were, respectively, arranged on the upper and lower edges of the section. Single-limb shear-resistance stirrups were arranged at distances of 100 mm in the longitudinal direction of the test beam, and the diameters of the other structural reinforcements were 8 mm. The mechanical properties of the reinforcement are shown in Table 3.

After pouring UHPC, the test beams were covered with plastic film for 2 days and then demolded, followed by steam curing for 3 days (temperature $\geq 90^\circ\text{C}$; relative humidity $> 90\%$). After steam curing, the beams were stored in a room for 28 days, then tensioned and grouted, and finally naturally cured until the test began.

3.3. Test Procedures and Instruments. The device and instruments used in this test are shown in Figure 11. A hydraulic Jack was used for grading single-point loading. At the initial stage, the loading was carried out at 50 kN per stage. After obvious cracks appeared, the loading was controlled by displacement until the specimens were destroyed. The test involved the following main stages:

- Load test: this was read by the pressure sensor arranged between the Jack and the reaction frame.
- Displacement test: all three test beams were equipped with five displacement sensors (the numbers are 0–4 from left to right).
- Strain test: the distribution of the strain gauges of the full beam is illustrated in Figure 12. Five longitudinal strain gauges were arranged on the top plate, and three longitudinal strain gauges were arranged on the bottom plate of a typical section to measure the

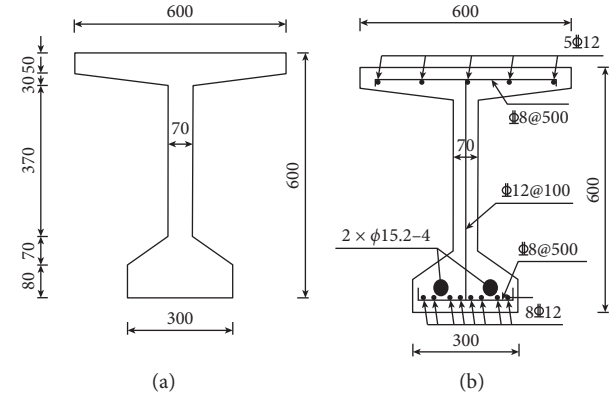


FIGURE 10: (a) Test beam section. (b) Longitudinal reinforcement layout (mm).

TABLE 3: Mechanical properties of reinforcement.

Mechanical property	Diameter	f_y (MPa)	f_{st} (MPa)	E_s (MPa)
Structural reinforcement	$\Phi 12$	384	542	210
Stirrup	$\Phi 8$	345	500	210
Longitudinal bar	$\Phi 8$	345	500	210
Prestressed reinforcement	$\Phi 15.2-4$	1820	1940	195

longitudinal strain of the top and bottom plates. Several strain rosettes were arranged symmetrically on both sides of the web to measure the web strain.

- Crack test: the width and length of the crack were measured by a crack observation instrument and ruler.

4. Test Results and Analysis

4.1. Shear Resistance. The test results are shown in Table 4, where V_{cr} and V_{max} are the cracking load and ultimate load of the test beam, respectively. When the shear-span ratio increased from 1.06 to 2.12, the bearing capacity of the beam decreased by 39.64%, and when the shear-span ratio increased from 2.12 to 3.19, the bearing capacity decreased by 4.58%, indicating that the shear-span ratio greatly influences the shear performance of UHPC beams, and its influence degree decreases upon increasing the shear-span ratio. The reason is that vertical compressive stress is generated at the support reaction and concentrated load, which reduces the main tensile stress of concrete, which then improves the shear capacity of the beam. When the shear-span ratio is small, the vertical compressive stress affects the whole shear-span area; however, the influence of the vertical compressive stress is gradually limited to the support reaction and

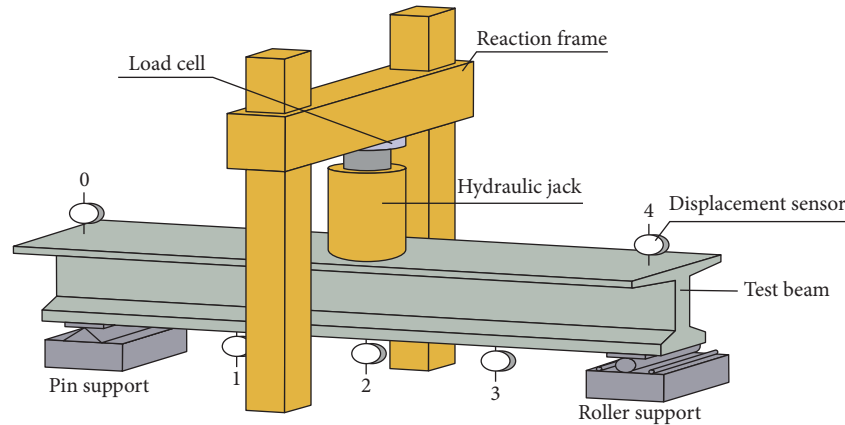


FIGURE 11: Experimental device and instruments.

concentrated load upon increasing the shear-span ratio, which weakens its effect. In addition, upon increasing the shear-span ratio, when the failure mode of the beam changed from inclined compression failure to diagonal tensile failure, that is, the bearing capacity changed from compressive strength control to tensile strength control, there was a significant decrease, but the specific impact degree requires further study.

4.2. Failure Modes and Crack Distributions. As depicted in Figure 13, three failure modes were observed in the three test beams, namely, inclined compression failure, shear compression failure, and diagonal tension failure.

The failure mode of beam L1 was inclined compression failure. When the load reached 945 kN, the first inclined crack appeared in the web of the right shear span. As the load increased, the crack increased continuously. At this time, the cracks on the left side of the beam appeared more densely, a series of approximately parallel oblique cracks formed at the connection line between the loading point and the support, and the inclination angles of these cracks were in the range of 37–57°. The concrete between the load point and the support was compressed into pieces when the load reached 2700 kN, some of the concrete peeled outward, and the beam was destroyed.

The failure mode of beam L2 was shear compression failure. The first diagonal crack appeared on the left side when loading to 302 kN. As the load increased, cracks appeared continuously on both sides of the webs. When the load reached 1000 kN, many dense diagonal cracks appeared on both sides, and the inclination angles of these cracks were in the range of 32–43°. When the load was increased to 1690 kN, a critical oblique crack between the support and the loading point appeared, and the inclination angle was about 41°. The sound of steel fiber tearing could be clearly heard, and the outer skin of the concrete was peeled off. The stirrup and the longitudinal bars successively yielded, and the concrete was crushed until the beam failed.

The failure mode of beam L3 was diagonal tension failure. When the load was increased to 805 kN, the first diagonal crack appeared on the right web, and the crack

developed continuously upon increasing the load. When the load reached 1045 kN, the crack width reached 0.21 mm. As the load continued to increase, many diagonal cracks appeared on both sides of the webs. The inclination angles of these cracks were within the range of 26–35°, and bending cracks began to appear in the bottom slab. When the beam approached failure, critical diagonal cracks appeared on the right side of the beam. The inclination angle was about 28°, the bending cracks of the bottom plate extended and widened, and horizontal tearing occurred at the junction of the top plate and the web until the beam broke.

Upon increasing the shear-span ratio, the inclination angle of the inclined crack of the beam decreased, and the failure mode also changed. When the beam underwent inclined compression failure, the shear bearing capacity was controlled by the compressive strength of concrete, so there was no steel fiber tearing phenomenon. When the beam underwent shear compression failure, the shear bearing capacity was controlled by the bite force between the compressive zone at the top of the detached body and the steel fiber at the inclined crack. The sound of steel fiber tearing could be clearly heard during the failure process. When the beam underwent diagonal tension failure, the shear bearing capacity was controlled by the tensile strength of concrete; however, due to the bridge effect of steel fiber, the tensile strength of the beam was improved, so the ultimate bearing capacity of beams L2 and L3 was similar. The compressive strength of UHPC concrete is much larger than the tensile strength, so the ultimate bearing capacity of beam L1 was much larger than that of beams L2 and L3.

4.3. Load-Displacement Curves. Figure 14 shows the load-displacement curves of the three beams. It can be seen that the stiffness of beam L1 was significantly greater than that of the other two beams. In the initial stage of loading, the curve slope changed slightly and approximately linearly, which indicates that the beam was in an elastic state. Then, the curve slope decreased significantly, showing a nonlinear change, which indicates that the structure underwent inelastic damage, and the beam was in an inelastic state. The overall changes of the three curves are relatively gentle,

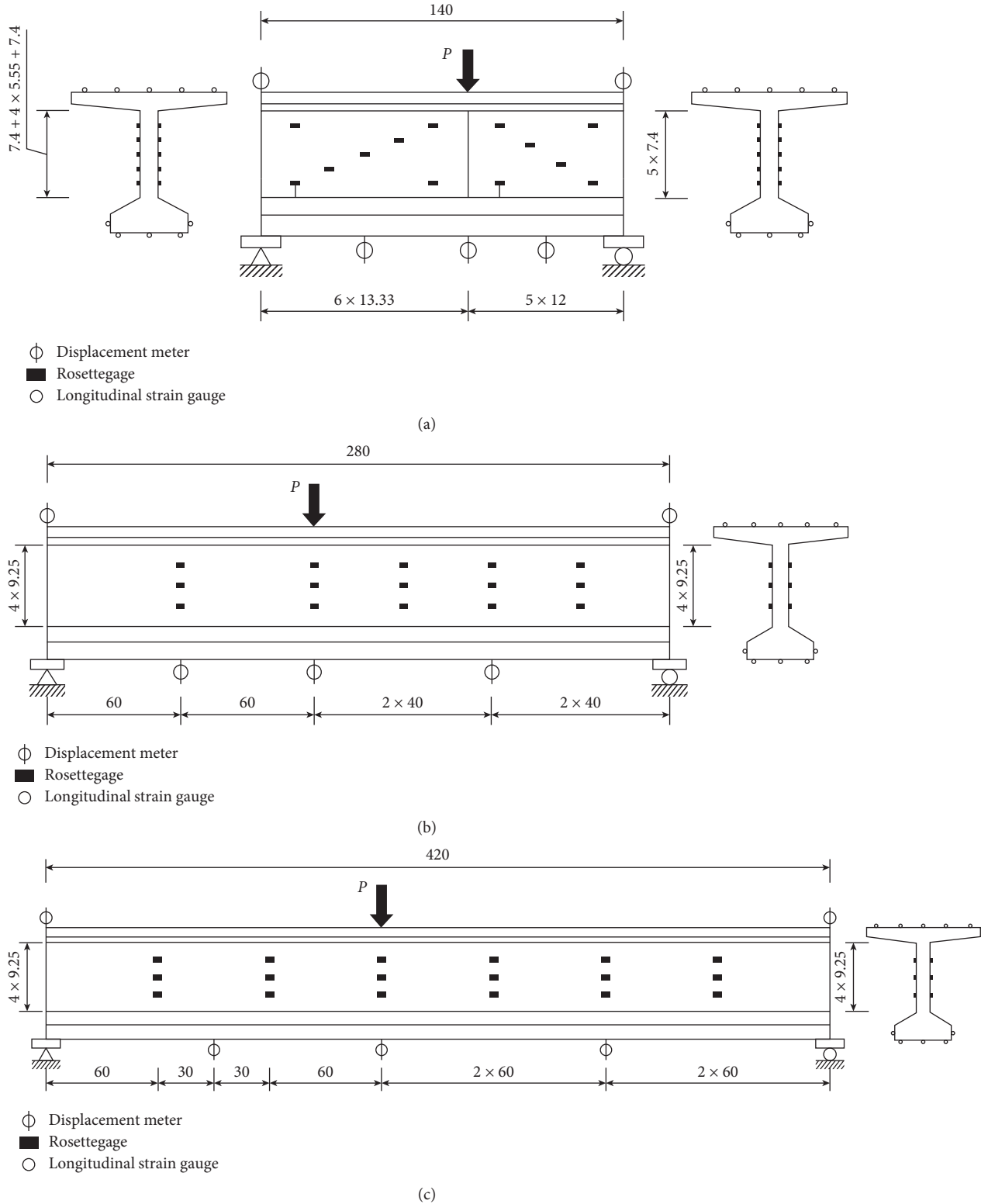


FIGURE 12: Positions of strain gauges. (a) L1, (b) L2, and (c) L3.

without obvious inflection points because the UHPC beams contain steel fiber, which can still bear tensile stress after cracking. The maximum displacements for beams L1, L2, and L3 were 6.7 mm, 13.1 mm, and 25.6 mm, respectively. The slope of the curve of beam L3 decreased the fastest,

which indicates that, upon increasing the shear-span ratio, the principal stress of the UHPC element changed from compressive to tensile, and the stiffness of the components decreased the fastest. This is because the shear-span ratio reflects the ratio of the bending moment and shear force of

TABLE 4: Shear-resistance test results.

Test beam	λ	V_{cr} (kN)	V_{max} (kN)	Failure mode
L1	1.06	945	2800	Inclined compression failure
L2	2.12	302	1690	Shear compression failure
L3	3.19	805	1622	Diagonal tension failure

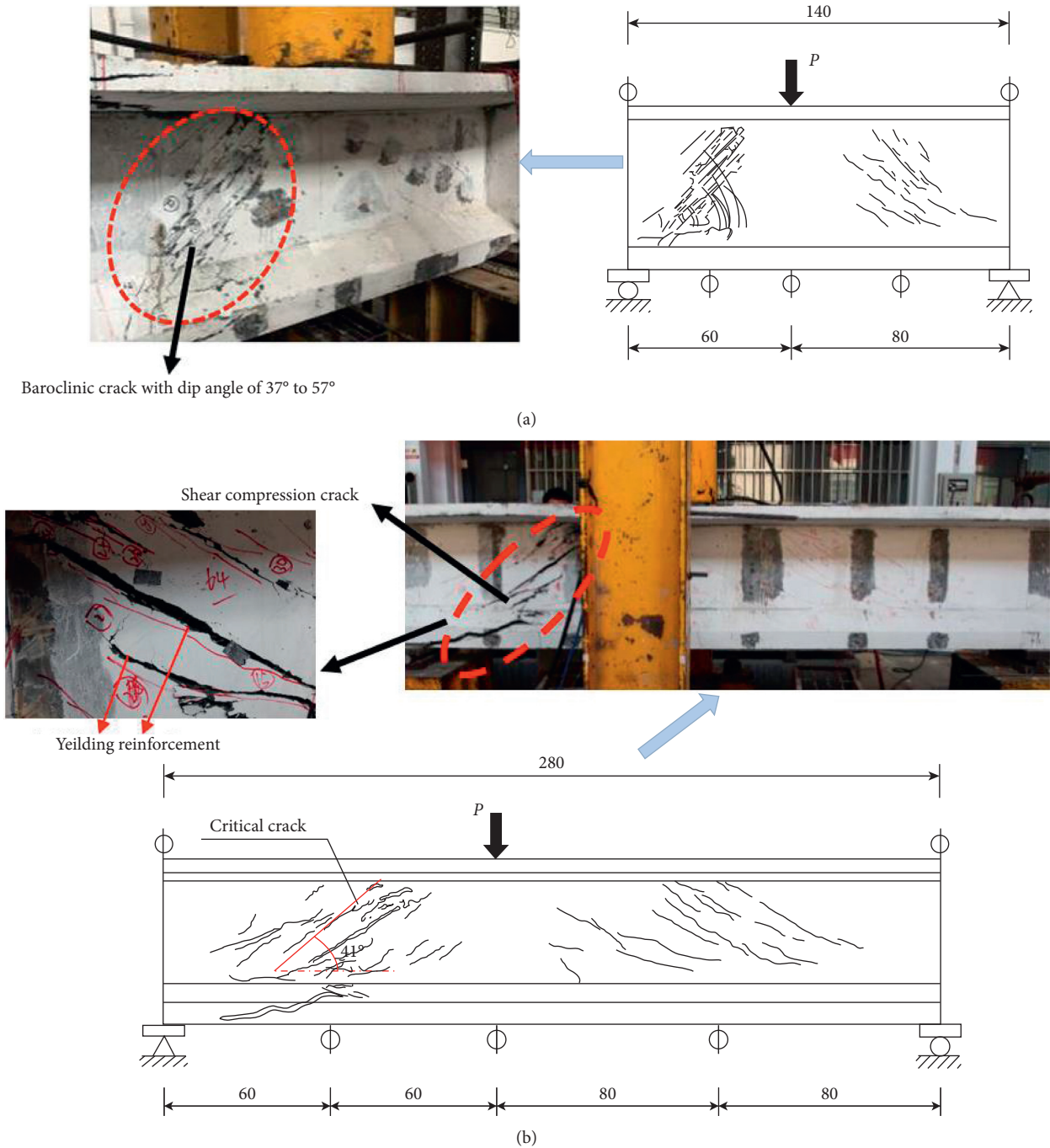


FIGURE 13: Continued.

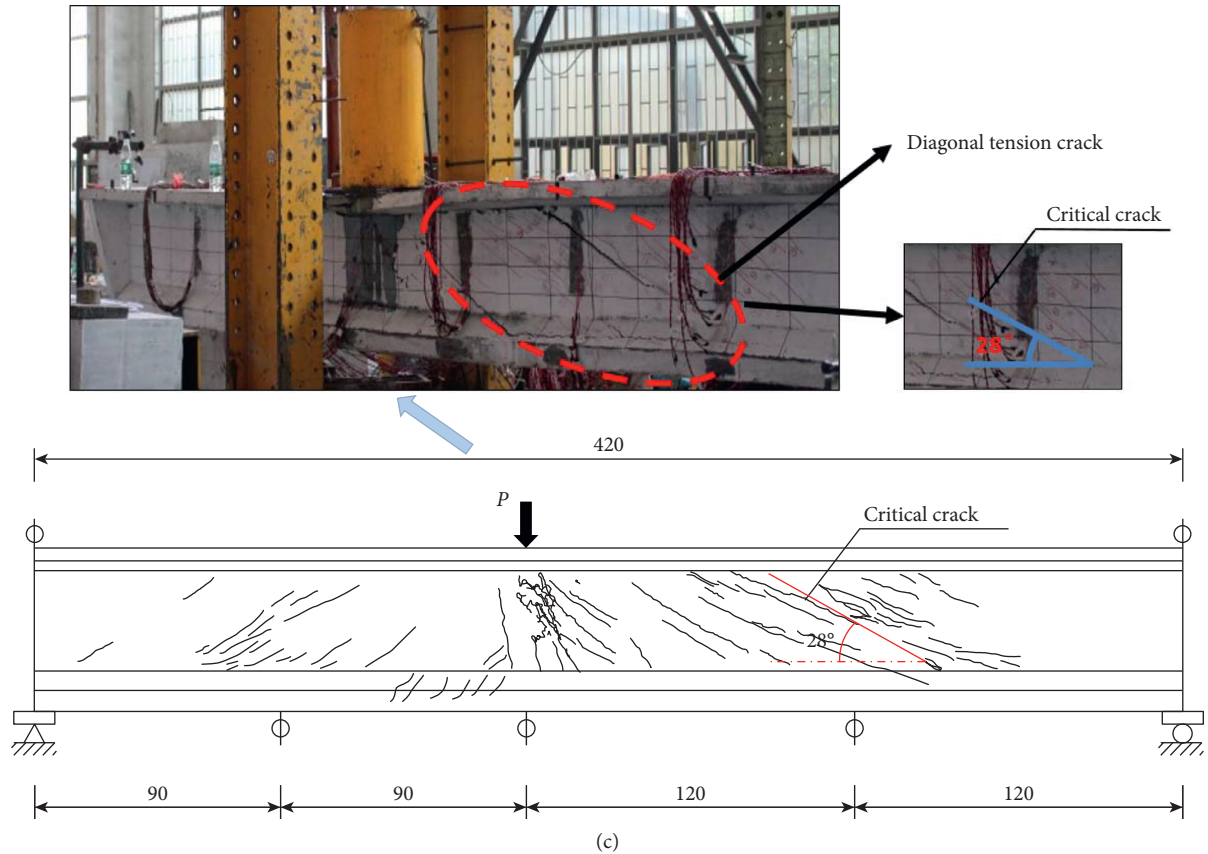


FIGURE 13: Failure modes of the test beams. (a) L1, (b) L2, and (c) L3.

the beam failure section under a concentrated load. When the shear force is the same, the larger the shear-span ratio, the smaller the effective inertia moment of the cross section after the formation of oblique cracks, resulting in a significant decrease in beam stiffness.

4.4. Load-Strain Relationship

4.4.1. Web Tensile Strain. Figure 15 shows the load-web tensile strain relationship of three beams. The growth trends of the web tensile strain of the three beams were basically the same before the appearance of cracks. The web of beam L1 cracked when the strain reached $410 \mu\epsilon$, and the load was 945 kN. The web of beam L2 cracked when the strain reached $812 \mu\epsilon$, and the load was 1408 kN. The web of beam L3 cracked when the strain reached $390 \mu\epsilon$, and the load was 805 kN. After cracking, the web tensile strain increased rapidly, among which the L2 beam grew the fastest.

4.4.2. Bottom Plate Tensile Strain. Figure 16 shows the load-bottom plate tensile strain relationship of the three beams. The bottom plate tensile strain increased linearly before cracking. The bottom plate of beam L1 cracked when the strain reached $631 \mu\epsilon$, and the load was 1544 kN. The bottom plate of beam L2 cracked when the strain reached $230 \mu\epsilon$, and the load was 302 kN. The bottom plate of beam L3 cracked

when the strain reached $383 \mu\epsilon$, and the load was 914 kN. After cracking, the bottom plate tensile strain increased rapidly. When the bottom plate tensile strain of beam L3 was about $2500 \mu\epsilon$, there were no data from the strain gauge due to the failure of the strain gauge at the bottom of the bending crack.

For the load-strain response, the data measured by strain gauges before cracking are reliable; however, after cracking, the distribution of cracks greatly influenced the strain test results. For example, the strain gauge across the cracks will record a larger strain, and the strain gauge not located across the cracks may even record a strain reduction due to cracking of the surrounding area; therefore, only the typical load-strain response is given here.

5. Calculation and Analysis of Shear Capacity

5.1. Calculation of Shear Capacity Based on Existing Specifications. At present, there are few design specifications for UHPC. The French specification [34], the Swiss specification [35], the “Highway Bridge specification” [36], and the “Technical Specification for High-Strength Concrete Structures” [37] were used to calculate the shear capacities of the test beams. The ratios of the test values to the calculated values are presented in Table 5, where V_{exp} indicates the test value and V_{cal} is the calculated value.

Table 5 shows that the measured values of the shear capacities of the three test beams were higher than the

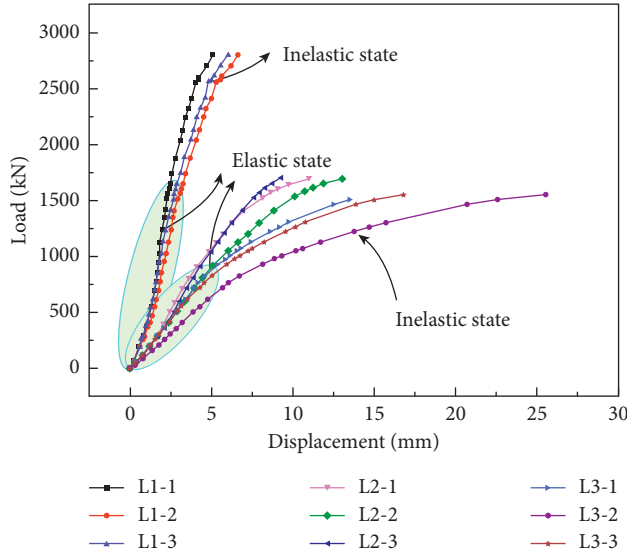


FIGURE 14: Load-displacement curves of the test beam.

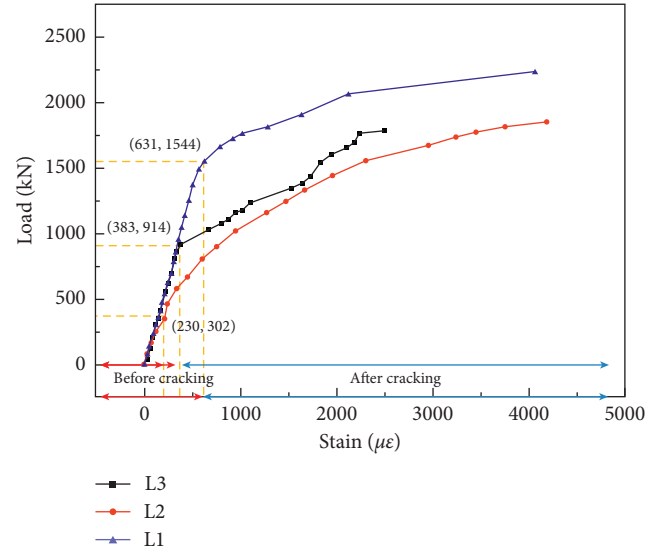


FIGURE 16: Load-bottom plate tensile strain relationship.

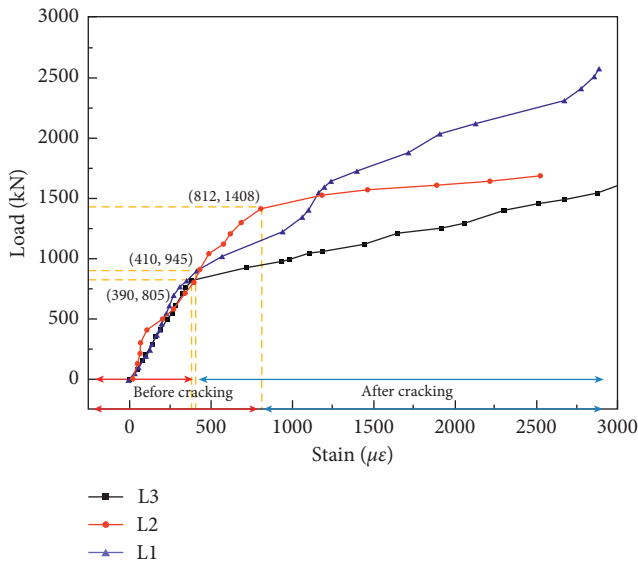


FIGURE 15: Load-wed tensile strain relationship.

calculated values. The smaller the shear-span ratio, the more obvious this difference. The main reasons for these discrepancies are as follows:

- Most specifications are proposed for rectangular beams, and the contribution of the flange part of T-shaped beams to the shear bearing capacity is not considered; thus, the calculations of the specifications are conservative
- The residual tensile strength after UHPC cracking contributes a larger proportion to the shear bearing capacity, and the values in the standard calculation are different from the actual values, resulting in calculation errors
- The impact of the shear-span ratio is not sufficiently considered in the specifications

5.2. Calculation Formula of the Shear Capacity of UHPC Beam. The MCFT models contain many calculation parameters and complex convergence conditions, and the shear capacity calculations in existing specifications are too conservative. To facilitate the engineering applications of UHPC beams, the test data from previous studies were collected for fitting [15, 18, 32, 38]. The influence of the concrete part, stirrup part, and prestressed reinforcement part on the shear bearing capacity of UHPC beams is considered, and the calculation formula of the shear bearing capacity is proposed. Each part of the formula takes into account the influence of the shear-span ratio and introduces its own calculation parameters. The specific formula is as follows:

$$V = V_c + V_s + V_p, \quad (26)$$

$$V_c = \left(\frac{3.42}{\lambda} - 0.38 \right) \alpha_1 \sqrt{f_c} b h_0, \quad (27)$$

$$V_s = (0.506\lambda - 0.18) f_{yv} \rho_{sv} b h_0, \quad (28)$$

$$V_p = \frac{0.41}{\lambda} N_{p0}, \quad (29)$$

where V_c , V_s , and V_p are the shear forces of the UHPC concrete, stirrups, and prestressed reinforcement, respectively; λ is the shear-span ratio, which has a value of 1.5 when the value is less than 1.5 and a value of 3 when the value is greater than 3; α_1 is the flange coefficient; f_{yv} and ρ_{sv} are the stirrup yield strength and stirrup ratio, respectively; N_{p0} is the resultant force of prestressed reinforcement and non-prestressed reinforcements when the normal stress of the calculated section of concrete is 0.

5.3. Comparison of Results Verification. To verify the correctness and applicability of the MCFT model and formula,

TABLE 5: Comparison between the test values and code calculated values.

Test beam	V_{exp}/V_{cal} [34]	V_{exp}/V_{cal} [35]	V_{exp}/V_{cal} [36]	V_{exp}/V_{cal} [37]
L1	2.79	3.42	5.45	2.41
L2	1.69	2.06	3.29	1.58
L3	1.59	1.98	3.16	1.66
Average value	2.02	2.49	3.97	1.88

TABLE 6: Comparison of experimental results and predicted values.

Specimen number	Test value (kN)	MCFT (kN)	Equation (26) (kN)	Theoretical/experimental	Formula/test
<i>This study</i>					
L1	2800	2470.0	2324	0.88	0.83
L2	1690	1811.4	1825.2	1.07	1.08
L3	1622	1811.4	1411.1	1.12	0.87
<i>Literature data</i>					
Ji et al. [18]					
L-2-100-a	556.0	552.5	487	0.99	0.88
L-3-100-a	410.0	415.6	290.8	1.01	0.71
L-4-100-a	360.0	363.4	301.8	1.01	0.84
L-1-100-a	755.0	756.5	695.5	1.00	0.92
L-2-200-a	500.0	515.5	457.5	1.03	0.92
L-2-150-a	507.0	517.9	493.8	1.02	0.97
Chen [38]					
B-2-60-90	320.0	330.5	385.2	1.03	1.20
B-2-60-180	285.0	308.7	368.7	1.08	1.29
B-2-30-90	314.0	310.0	338.6	0.99	1.08
B-2-30-180	246.0	251.0	308.9	1.02	1.26
B-2-0-90	287.5	246.5	310.3	0.86	1.08
B-2-0-180	240.0	239.8	276.3	1.00	1.15
B-3-60-90	285.5	291.8	291.6	1.02	1.02
B-1-60-90	370.0	359.4	494.6	0.97	1.34
<i>Total mean</i>				1.01	1.03
<i>Coefficient of variation</i>				0.061	0.17

the calculated results were compared and analyzed with previously published experimental data, as presented in Table 6.

Table 6 shows that the values calculated using the MCFT model and fitting formula agree well with the experimental values. The concept of the formula is clear, and the calculation process is simple. These results indicate that the MCFT model and fitting formula can be used to analyze and calculate the shear capacity of UHPC beams.

5.4. Discussion on the Feasibility and Design Proposal.

In the MCFT analysis model proposed in this paper, to simplify the calculation, ε_x in the shear calculation was taken as the longitudinal strain at half the height of the section in the bending calculation. The applicability of this method to the actual structure needs further discussion. In the shear design of a UHPC beam structure, when the shear-span ratio is small, the influence of the UHPC tensile strength can be ignored or used as a safety reserve in shear design. When the shear-span ratio is large, the contribution of the UHPC tensile strength to beam shear should be considered; therefore, to establish a complete UHPC shear calculation

theory, more shear tests are still needed to lay the foundation for a theoretical analysis.

6. Conclusions

The following conclusions can be drawn according to the above research:

- (1) In this paper, the shear analysis model of UHPC-T beams based on the modified compression field theory fully considered changes in the shear performance of UHPC structures under the combined action of bending and shearing. The comparison between the calculated and experimental results proved the rationality of the assumptions in the theory, indicating that the established model was suitable for predicting the shear bearing capacity of UHPC beams.
- (2) The shear capacity of the UHPC beam decreased upon increasing the shear-span ratio, but the extent of the decrease gradually slowed. In this paper, when the shear-span ratio changed from 1.04 to 2.12, the shear bearing capacity decreased greatly, whereas the decrease was very small when the shear-span ratio changed from 2.12 to 3.19.

- (3) The shear-span ratio affects the failure mode of beams. When the shear-span ratio is 1.06, the failure mode is inclined compression failure. When the shear-span ratio is 2.12, the failure mode is shear compression failure. When the shear-span ratio is 3.19, the failure mode is diagonal tension failure.
- (4) The shear capacity of the UHPC beam calculated by existing specifications led to conservative results; the smaller the shear-span ratio, the more obvious the difference. The simplified prediction formula proposed in this paper based on the MCFT model and existing test data fully considered the influence of the shear-span ratio. The calculation process was simple and was verified by previously published experimental results, which can provide a reference for the shear design of UHPC beams in practical engineering applications.

Data Availability

The data used to support the findings of this study are available from the corresponding author upon request.

Conflicts of Interest

The authors declare that there are no conflicts of interest regarding the publication of this paper.

Acknowledgments

This research was funded by the National Natural Science Foundation of China (no. 51278183), scientific research project of Shaanxi Provincial Department of Transportation (no. 14-18k), and special funds for Basic Scientific Research Fees of Central Universities (no. 310821161102).

References

- [1] Y. L. Voo, S. J. Foster, and C. C. Voo, "Ultrahigh-performance concrete segmental bridge technology: toward sustainable bridge construction," *Journal of Bridge Engineering*, vol. 20, no. 5, Article ID B5014001, 2015.
- [2] I.-H. Yang, J. Park, T. Q. Bui, K.-C. Kim, C. Joh, and H. Lee, "An experimental study on the ductility and flexural toughness of ultrahigh-performance concrete beams subjected to bending," *Materials*, vol. 13, no. 10, Article ID 2225, 2020.
- [3] G. S. Ryu, S. T. Kang, J. J. Park, K. T. Koh, and S. W. Kim, "Mechanical behavior of UHPC (ultra high performance concrete) according to hybrid use of steel fibers," *Advanced Materials Research*, vol. 287–290, pp. 453–457, 2011.
- [4] M. Shafieifar, M. Farzad, and A. Azizinamini, "Experimental and numerical study on mechanical properties of ultra high performance concrete (UHPC)," *Construction and Building Materials*, vol. 156, pp. 402–411, 2017.
- [5] D.-Y. Yoo and N. Banthia, "Mechanical properties of ultra-high-performance fiber-reinforced concrete: a review," *Cement and Concrete Composites*, vol. 73, pp. 267–280, 2016.
- [6] J. Wang, J. Liu, Z. Wang, T. Liu, J. Liu, and J. Zhang, "Cost-Effective UHPC for accelerated bridge construction: material properties, structural elements, and structural applications," *Journal of Bridge Engineering*, vol. 26, no. 2, Article ID 04020117, 2021.
- [7] H. Chu, F. Wang, L. Wang, T. Feng, and D. Wang, "Mechanical properties and environmental evaluation of ultra-high-performance concrete with aeolian sand," *Materials*, vol. 13, no. 14, Article ID 3148, 2020.
- [8] M. Zhou, W. Lu, J. Song, and G. C. Lee, "Application of ultra-high performance concrete in bridge engineering," *Construction and Building Materials*, vol. 186, pp. 1256–1267, 2018.
- [9] B. A. Tayeh, B. H. A. Bakar, M. A. M. Johari, and Y. L. Voo, "Utilization of ultra-high performance fibre concrete (UHPFC) for rehabilitation—a review," *Procedia Engineering*, vol. 54, pp. 525–538, 2013.
- [10] B. A. Tayeh, B. H. Abu Bakar, and M. A. Megat Johari, "Characterization of the interfacial bond between old concrete substrate and ultra high performance fiber concrete repair composite," *Materials and Structures*, vol. 46, no. 5, pp. 743–753, 2013.
- [11] K. W. Ng, J. Garder, and S. Sritharan, "Investigation of ultra high performance concrete piles for integral abutment bridges," *Engineering Structures*, vol. 105, pp. 220–230, 2015.
- [12] B. A. Graybeal, *Material Property Characterization of Ultra-high Performance Concrete*, US Department of Transportation, Washington, DC, USA, 2006.
- [13] M. Schmidt, "Sustainable building with ultra-high-performance concrete (uhpc)-coordinated research program in Germany," in *Proceedings of the Third International Symposium on UHPC and Nanotechnology for High Performance Construction Materials*, vol. 17, Kassel, Germany, March 2012.
- [14] H. Almansour and Z. Lounis, "Innovative design approach of precast-prestressed girder bridges using ultra high performance concrete," *Canadian Journal of Civil Engineering*, vol. 37, no. 4, pp. 511–521, 2010.
- [15] Y. L. Voo, S. J. Foster, and R. I. Gilbert, "Shear strength of fiber reinforced reactive powder concrete prestressed girders without stirrups," *Journal of Advanced Concrete Technology*, vol. 4, no. 1, pp. 123–132, 2006.
- [16] Y. L. Voo, W. K. Poon, and S. J. Foster, "Shear strength of steel fiber-reinforced ultra-high performance concrete beams without stirrups," *Journal of Structural Engineering*, vol. 136, no. 11, pp. 1393–1400, 2010.
- [17] T. T. Ngo, J. K. Park, S. Pyo, and D. J. Kim, "Shear resistance of ultra-high-performance fiber-reinforced concrete," *Construction and Building Materials*, vol. 151, pp. 246–257, 2017.
- [18] W. Y. Ji, B. Ding, and M. Z. An, "Experimental Study on the shear capacity of reactive powder concrete t-beams," *China Railway Science*, vol. 32, no. 5, pp. 38–42, 2011.
- [19] W. Ji, W. Li, M. An, and L. Zhu, "Shear capacity of t-section girders made of reactive powder concrete," *Journal of Bridge Engineering*, vol. 23, no. 7, Article ID 04018041, 2018.
- [20] A. Marí, A. Cladera, J. Bairán, E. Oller, and C. Ribas, "Shear-flexural strength mechanical model for the design and assessment of reinforced concrete beams subjected to point or distributed loads," *Frontiers of Structural and Civil Engineering*, vol. 8, no. 4, pp. 337–353, 2014.
- [21] W. F. Chen, *Plasticity in Reinforced Concrete*, J. Ross Publishing, Plantation, FL, USA, 2007.
- [22] W. Ritter, *Die Bauweise Hennebique*, Schweizerische Bauzeitung, Zurich, Switzerland, 1899.
- [23] T. Xu, Z. Zhou, R. Yan et al., "Real-time monitoring method for layered compaction quality of loess subgrade based on hydraulic compactor reinforcement," *Sensors (Switzerland)*, vol. 20, no. 15, pp. 4288–4320, 2020.

- [24] F. J. Vecchio and M. P. Collins, "The modified compression-field theory for reinforced concrete elements subjected to shear," *ACI Structural Journal*, vol. 83, pp. 219–231, 1986.
- [25] F. J. Vecchio and M. P. Collins, "Predicting the response of reinforced concrete beams subjected to shear using modified compression field theory," *ACI Structural Journal*, vol. 85, pp. 258–268, 1988.
- [26] Association Canadienne de Normalization, *CSA A23.3-04: Design of Concrete Structures*, Canadian Standards Association, Mississauga, Canada, 2004.
- [27] L. R. F. D. Aashto, *AASHTO LRFD-2007: Bridge Design Specifications*, American Association of State Highway Transportation officials, Washington, DC, USA, 2007.
- [28] C. K. Crane, *Shear and Shear Friction of Ultra-High Performance Concrete Bridge Girders*, Civil Engineering Division, Georgia Institute of Technology, Atlanta, GA, USA, 2010.
- [29] X. W. Liang and Z. Y. Wang, "Shear capacity analysis of ultra-high-performance concrete beams base on the improved MCFT," *Industrial Construction*, vol. 49, no. 1, pp. 63–68, 2019.
- [30] F. Baby, P. Marchand, M. Atrach, and F. Toutlemonde, "Analysis of flexure-shear behavior of UHPFRC beams based on stress field approach," *Engineering Structures*, vol. 56, pp. 194–206, 2013.
- [31] J. Yang and Z. Fang, "Research on stress-strain of ultra high performance concrete beams," *Concrete*, vol. 7, pp. 11–15, 2008.
- [32] Z. Zhang, X. D. Shao, W. G. Li et al., "Axial tensile behavior test of ultra high performance concrete," *China Journal of Highway and Transport*, vol. 28, no. 8, pp. 50–58, 2015.
- [33] L. F. Li, X. Fan, and X. W. Shi, "Flexural behavior of a large-scale prestressed UHPC tee team," *China Civil Engineering Journal*, vol. 51, no. 5, pp. 88–98, 2018.
- [34] AFGC, *Ultra High Performance Fiber Reinforced Concretes*, Association Française de Genie Civil (AFGC), Paris, France, 2013.
- [35] SIA, *SIA2052: Ultra High Performance Fiber Reinforced Cement-Based Materials (UHPFRC)-materials, Design and Execution*, SIA, Zurich, Switzerland, 2016.
- [36] Ministry of Transport of the People's Republic of China, *JTG 3362-2018: Specifications for Design Of Highway Reinforced Concrete and Prestressed Concrete Bridge and Culverts*, China Communications Press, Beijing, China, 2018.
- [37] China Engineering Construction Standardization Association, *CECS104-99: Technical Specification for High-Strength Concrete Structures*, China Planning Press, Beijing, China, 1999.
- [38] B. Chen, "Study on the shear strength of prestressed RPC girders," Master thesis, Hunan University, Changsha, China, 2007.